VOL. 11, NO. 3, FEBRUARY 2016 ISSN 1819-6608
ARPN Journal of Engineering and Applied Sciences

www.arpnjournals.com

NUMERICAL CALCULATION OF PARTICLE MOTION IN COLD GAS DYNAMIC SPRAY

A. N. Ryabinin
Saint-Petersburg State University, St. Petersburg, Russia
E-Mail: a.ryabinin@spbu.ru

ABSTRACT

The calculation of the velocity and temperature of solid particles in the process of cold gas dynamic spraying is considered. The movement of the carrier gas in the de Laval nozzle and in the space between the nozzle exit and the substrate surface is determined by one-dimensional isentropic approach and by CFD method that comprising a solution of Euler and Reynolds Averaged Navier-Stokes (RANS) equations using a commercial package Ansys CFX. Particle velocity and particle temperature are obtained as a functions of particle diameter and input pressure. In the nozzle similar results are obtained by using a one-dimensional isentropic approach and the solution of the Euler equations. Calculated velocity of the particle is slightly greater than the velocity obtained by solutions of the RANS equations. For small particles of 1 micron in diameter, in the space between the nozzle exit and the substrate surface there are the large speed reduction and large particle heating due to of the bow shock near the substrate.

Keywords: cold gas dynamic spray, computational fluid dynamics, two-phase flow, solid particle, velocity, temperature.

INTRODUCTION

Cold gas dynamic spraying (CGDS or cold spray) is a process in which powder particles of spraying material are involved in high-speed gas flow. Particles accelerate in the gas stream and impact with the substrate material to form a coating [1 - 3]. Carrier gas is accelerated up to supersonic velocities through converging-diverging de Laval nozzle. Properties of the deposited coating and the deposition efficiency are determined by the speed and temperature of the particles at the time of impact [4 -7] and by substrate temperature [8, 9].

Most researchers separates the calculations of particle speed and temperature into two stages. In the first step, parameters of the gas are calculated in the nozzle and in the space between the nozzle and the substrate surface. In the second stage, the calculation of particle velocity and temperature is performed. It is usually assumed that the particle concentration is so low that particles have no influence on the characteristics of the gas flow [10 - 26]. Calculation of gas flows is carried out either based on one-dimensional isentropic approximation [10 - 12], or by Computational Fluid Dynamics (CFD) methods [12 - 28].

Basics of one-dimensional isentropic method of gas velocity calculation in Laval nozzle are presented in papers [3 - 5]. The application of this method of calculation gives some overestimated values for the particle velocities, because there is thick boundary layer near the nozzle wall, so the one-dimensional approximation is not valid. However, the correction, proposed in papers [12, 29, 30] leads to the fact that the estimation of the particle velocity becomes accurate.

Most of the CFD calculations were performed using the Fluent commercial software. The Lagrangian Discrete Phase Modeling (DPM) algorithm is implemented in Fluent. Thus, the calculation of the gas motion and the calculation of particle trajectory and particle velocity can be carried out sequentially by Fluent [12, 17 - 28].

The flow in De Laval nozzle in the case of high concentration of particles is not adiabatic and isentropic because there is heat and momentum transfer between the gas and particles. Earlier [31] we proposed one-dimensional non-isentropic method of calculation of gas parameters in De Laval nozzle.

In this paper, we propose low concentration of particles and use CFD method for calculation of gas parameters. We analyze the dependence of particle velocity and temperature on particle size and input pressure.

MATHEMATICAL MODEL OF PARTICLE MOTION

Equations of motion of a single particle (1) under the acting of aerodynamic force is taken from the [6, 7].

$$\frac{dv_p}{dt} = \frac{3}{4} C_D \frac{\rho}{\rho_p} \frac{(u - v_p)|u - v_p|}{d},$$
$$\frac{dx}{dt} = v_p, \qquad (1)$$
$$\frac{dT_p}{dt} = \frac{6\,\mathrm{Nu}\,k}{d^2 \rho_p c}(T - T_p),$$

where u, ρ and T are velocity, density and temperature of the gas, v_p, ρ_p, T_p, d, c are velocity, density, temperature, diameter and specific heat of the particle, Nu is Nusselt number, which depends on Reynolds number Re, Prandtl

VOL. 11, NO. 3, FEBRUARY 2016 ISSN 1819-6608
ARPN Journal of Engineering and Applied Sciences

number Pr and Mach number M [27], C_D is drag coefficient, k is thermal conductivity,

$$\mathrm{Re} = \frac{\rho\,|u - v_p|\,d}{\mu}, \quad \mathrm{M} = \frac{|u - v_p|}{a},$$

where μ is the gas viscosity, a is sound velocity.

Expression for Nusselt number was taken from [27]:

$$\mathrm{Nu} = 2 + 0.44\,\mathrm{Re}^{1/2}\,\mathrm{Pr}^{1/3}\exp(0.1 + 0.872\mathrm{M}).$$

This expression is only valid for M > 0.24 and $T > T_p$. In all other cases, the Nusselt number does not depend on Mach number:

$$\mathrm{Nu} = 2 + 0.44\,\mathrm{Re}^{1/2}\,\mathrm{Pr}^{1/3}.$$

Expressions for drag coefficient C_D were taken from Henderson paper [32]. Drag coefficient C_D is the function of Mach number M and Reynolds number Re: $C_D = C_D(\mathrm{M}, \mathrm{Re})$.

If M ≤ 1.0 then

$$C_D = 24\left[\mathrm{Re} + S\left\{4.33 + \frac{3.65 - 1.53\Omega}{1 + 0.363\Omega}\exp\left(-0.247\frac{\mathrm{Re}}{S}\right)\right\}\right]^{-1} + \exp\left(-\frac{0.5\mathrm{M}}{\sqrt{\mathrm{Re}}}\right)\left[\frac{4.5 + 0.38\Phi}{1 + \Phi} + 0.1\mathrm{M}^2 + 0.2\mathrm{M}^8\right] + \left[1 - \exp\left(-\frac{\mathrm{M}}{\mathrm{Re}}\right)\right]0.6S, \quad (2)$$

$$\Omega = T_p - T, \quad S = \mathrm{M}\sqrt{\gamma/2}, \quad \Phi = 0.03\,\mathrm{Re} + 0.48\sqrt{\mathrm{Re}}.$$

If M ≥ 1.75 then

$$C_D = \frac{0.9 + \frac{0.34}{\mathrm{M}^2} + 1.86\sqrt{\frac{\mathrm{M}}{\mathrm{Re}}}\left[2 + \frac{2}{S^2} + \frac{1.058\Omega}{S} - \frac{1}{S^4}\right]}{1 + 1.86\sqrt{\frac{\mathrm{M}}{\mathrm{Re}}}}. \quad (3)$$

If 1.0 ≤ M ≤ 1.75 then:

$$C_D = C_D(1, \mathrm{Re}) + \frac{4}{3}(\mathrm{M} - 1)\left[C_D(1.75, \mathrm{Re}) - C_D(1, \mathrm{Re})\right]. \quad (4)$$

CFD METHOD

To calculate the motion of the particle using system of equations (1) it is necessary to know the velocity u and temperature T of the gas. For determination u and T we used both CFD method and one-dimensional isentropic calculations. Our CFD calculations were performed using the Ansys CFX commercial software [33]. On the inflow boundary the input pressure p_o is set. On the outflow boundary the average static pressure p_∞ is given. The slip (Euler equations) or no-slip condition (RANS equations) and vanishing flux of heat are used on the wall surface.

Solutions of Euler equations and Reynolds-averaged Navier-Stokes (RANS) equations are obtained with Ansys CFX - 13 finite volume solver [33] based on high-resolution discretization scheme [34]. Implicit second-order accurate backward Euler scheme is used to solve for time steps. The standard model of turbulence k-ω SST [35] is used in solutions of RANS equations. We considered axisymmetric flow in the convergent-divergent nozzle and in the space between nozzle exit and substrate. The sketch of the computational domain is presented in Figure-1.

In the solution of RANS equations the mesh was fined near the nozzle wall and near the substrate surface. The non-dimensional thickness of the first mesh layer y^+ is less than 1. Fragment of the mesh near the nozzle wall is shown in the Figure-1 *b*). The mesh for Euler equations has 89,118 elements. Most of the solutions of RANS equations are obtained with the mesh with 218,634 elements. However, a few calculations are carried out with 107,727 elements. Calculations demonstrated the independence of the results on mesh size.

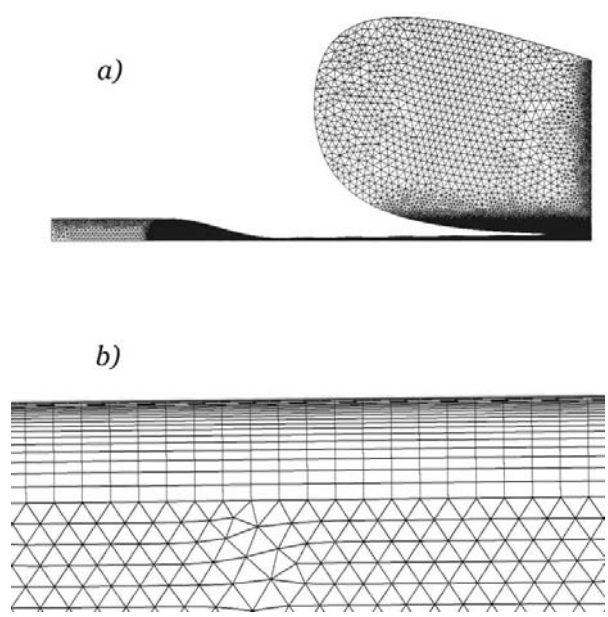

Figure-1. Sketch of the mech. *a*) Common view of computational domain. *b*) Fragment of the mesh near the wall of the nozzle.

VOL. 11, NO. 3, FEBRUARY 2016 ISSN 1819-6608
ARPN Journal of Engineering and Applied Sciences

www.arpnjournals.com

CALCULATIONS

The nozzle has a circular cross-section, the length of the converging part is equal to 50 mm and length of diverging part is equal to 120 mm. Before converging part there is cylindrical part. The length of cylindrical part is equal to 0.05 m. The nozzle had the throat of 2.67 mm in diameter. Exit diameter of diverging part was equal to 5.3 mm. We calculated the flight of copper particles, injected across the inlet part of the nozzle at the distance from the nozzle input x_o = 0.07 m. The throat of the nozzle is at the distance from the nozzle input x_t = 0.1 m. The nozzle exit is at the distance from the nozzle input x_e = 0.22 m. The substrate surface is situated at x_s = 0.24 m. The diameter of particles d was in the range from 1 μm to 125 μm. The inlet pressure p_o varied from 15 bar to 30 bar, inlet temperature T_o = 773 K. The carrier gas was air. Specific heat of air at constant pressure is equal to 1004.4 J / (kg K). Molar mass is equal to 28.96 kg/kmol. We use the Sutherland formula for molecular viscosity. We considered the particle flight near the axis of the nozzle. Initial particle velocity was equal to zero, initial particle temperature was equal 20ºC.

System of equations (1) was solved by fourth-order Runge-Kutta method. Code was written in Pascal.

The solutions of RANS equations demonstrated that there is thick boundary layer inside the nozzle. In contrast, the one-dimensional isentropic approximation and the solution of the Euler equations do not predict the existence of the boundary layer. The system of shock waves between the nozzle and the substrate in the solutions of RANS equations is also different from the system that gives the Euler equations. Figure-2 presents the system of shock waves between the nozzle and the substrate in the case of RANS equations.

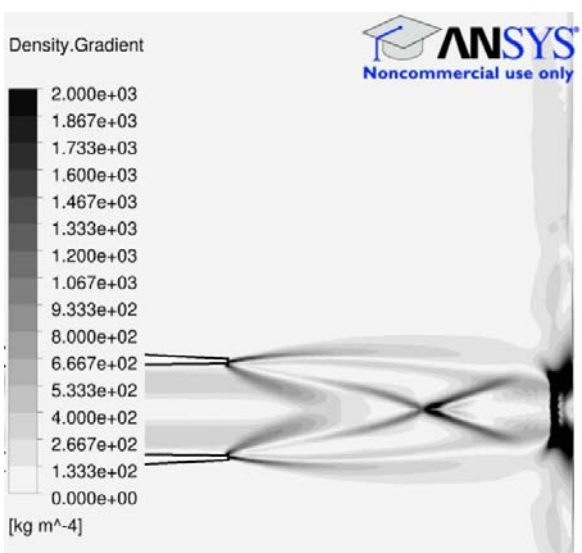

Figure-2. Solution of RANS equations. Density gradient image of the flow between the nozzle exit and the substrate. Input pressure p_o = 30 bar.

The bow shock near the sample surface significantly affects on the rate and temperature of the particle.

Figure-3 demonstrates the dependence of particle velocity on distance from the nozzle input at input pressure p_o = 30 bar. Gas velocity and temperature are calculated by three methods. One can see that one-dimensional isentropic approximation and solution of Euler equations give the same results inside the nozzle. Solution of RANS equations gives somewhat smaller particle velocity.

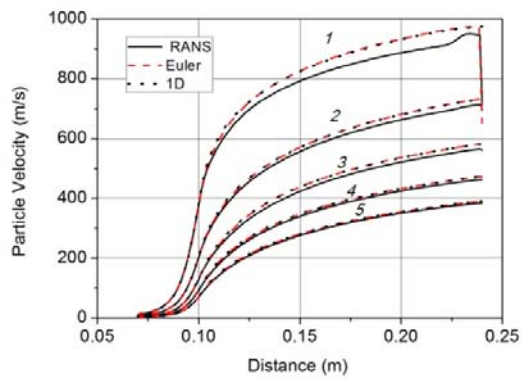

Figure-3. Particle velocity as a function of a distance from nozzle input. Input pressure p_o = 30 bar. *1* - d = 1 μm, *2* - d = 8 μm, *3* - d = 27 μm, *4* - d = 64 μm, *5* - d = 125 μm.

A significant deceleration of small particles occurs in the final stage of flight between the bow shock and the substrate surface. One can see in Figure-4 that distance between bow shock and substrate surface for RANS equations is less than for Euler ones.

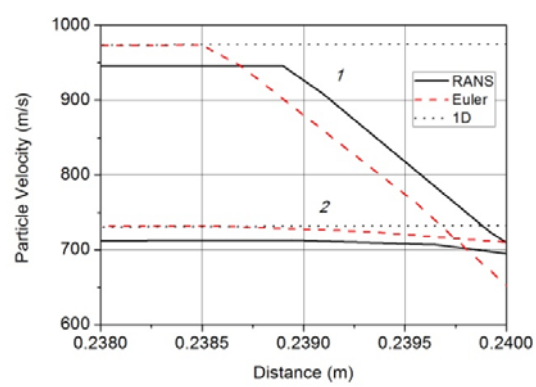

Figure-4. Particle velocity as a function of a distance from nozzle input near substrate surface. Input pressure p_o = 30 bar. *1* - d = 1 μm, *2* – d = 8 μm.

VOL. 11, NO. 3, FEBRUARY 2016 ISSN 1819-6608
ARPN Journal of Engineering and Applied Sciences

www.arpnjournals.com

Similar dependences of particle velocity on distance from the nozzle exit exist for other input pressure. Figure-5 shows this dependence at input pressure p_o = 15 bar.

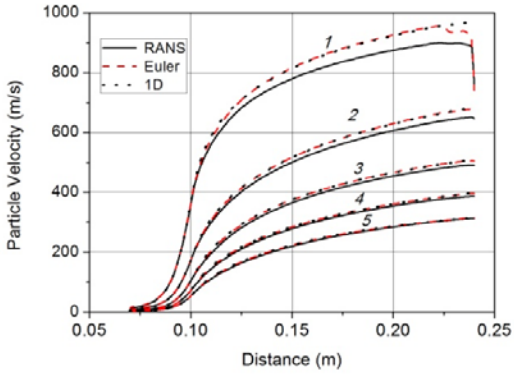

Figure-5. Particle velocity as a function of a distance from nozzle input. Input pressure p_o = 15 bar. *1* - *d* = 1 μm, *2* - *d* = 8 μm, *3* - *d* = 27 μm, *4* - *d* = 64 μm, *5* - *d* = 125 μm.

Deceleration of the small particle at the last stage of the flight depends on input pressure p_o. Figure-6 illustrates the dependence of impact particle velocity on input pressure.

In general, particle velocity rises if input pressure increases. However, deceleration of particle with diameter *d* = 1 μm rises too, and resulting particle velocity with diameter *d* = 1 μm decreases with increasing of input pressure. At p_o = 30 bar impact velocity of particle with diameter *d* = 1 μm is than impact velocity of particle with diameter *d* = 8 μm. This phenomenon can be explained by the change of shock configuration. Input pressure affects the configuration of the shock waves and intensity of the bow shock especially.

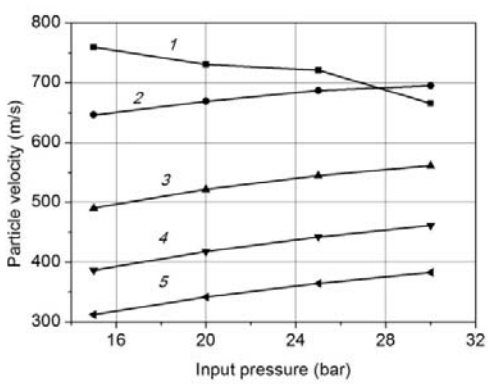

Figure-6. Particle velocity near substrate as a function of the input pressure. *1* - *d* = 1 μm, *2* - *d* = 8 μm, *3* - *d* = 27 μm, *4* - *d* = 64 μm, *5* - *d* = 125 μm.

Figure-7 shows the change of particle velocity in the space between the nozzle exit and the substrate surface. While small particles are significantly decelerated, larger particles are slightly accelerated.

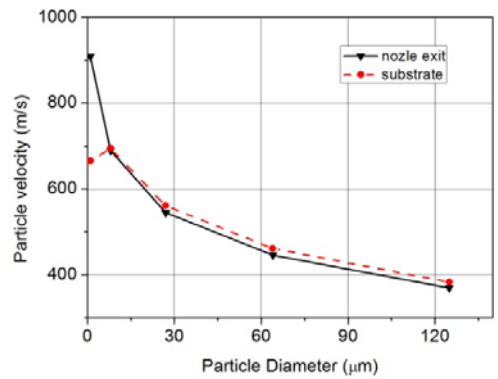

Figure-7. Particle velocity at the nozzle exit and near the substrate as a function of the particle diameter *d*. Input pressure p_o = 30 bar.

Figure-8 presents the dependence of the particle temperature on a distance from the nozzle input. Temperature of the smallest particle close on the gas temperature.

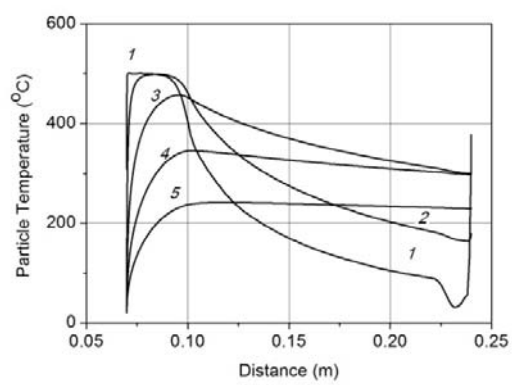

Figure-8. Particle temperature as a function of a distance from nozzle input. Input pressure p_o = 30 bar. *1* - *d* = 1 μm, *2* - *d* = 8 μm, *3* - *d* = 27 μm, *4* - *d* = 64 μm, *5* - *d* = 125 μm.

In converging part of the nozzle small particle is heated and then is cooled. The temperature of larger particle does not reach the temperature of the gas in converging part. In diverging part of the nozzle particles of any sizes are cooled. At the nozzle exit the medium particles with diameter *d* = 27 μm have the maximum temperature.

Figure-9 illustrates the change of particle temperature in the space between the nozzle exit and the

substrate surface. While small particles are significantly heated, larger particles are slightly cooled.

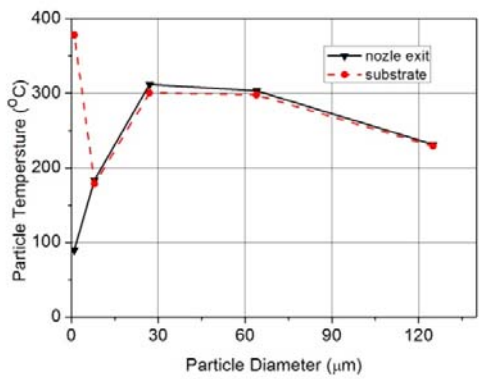

Figure-9. Particle temperature at the nozzle exit and near the substrate as a function of the particle diameter *d*. Input pressure p_o = 30 bar.

CONCLUSIONS

In the nozzle, similar results are obtained by using a one-dimensional isentropic approach and the solution of the Euler equations. Calculated velocity of the particle is slightly greater than the velocity obtained by solutions of the RANS equations. This phenomenon can be explained by existence of thick boundary layer near the nozzle wall. If input pressure increases particle velocity rises at the exit of the nozzle. However, in the space between nozzle and substrate there is the system of shock waves. If input pressure increases shock configuration changes. Deceleration effect of the shocks leads to decreasing of particle velocity for small particles.

For small particles of 1 micron in diameter, in the space between the nozzle exit and the substrate surface there are the large speed reduction and large particle heating due to of the bow shock near the substrate.

ACKNOWLEDGEMENT

Studies were performed using computing resources of Resource Center "Computing center of St. Petersburg State University" (http://cc.spbu.ru).

REFERENCES

[1] Papyrin A., Kosarev V., Klinkov S., Alkhimov A., Fomin V. 2007. Cold spray technology, Elsevier Science, Amsterdam. p. 336.

[2] Irissou E., Legoux J.-G., Moreau C., Ryabinin A.N., Jodoin B. 2008. Review on cold spray process and technology: Part I. Intellectual property. Journal of Thermal Spray Technology. 17(4): 495-516.

[3] Dykhuizen R.C., Smith M.F. 1998. Gas dynamic principles of cold spray. Journal of Thermal Spray Technology. 7(2): 205-212.

[4] Schmidt T., Assadi H., Gartner F., Richter H., Stoltenhoff T., Kreye H., Klassen T. 2009. From particle acceleration to impact and bonding in cold spraying. Journal of Thermal Spray Technology. 18(5-6): 794-808.

[5] Assadi H., Schmidt T., Richter H., Kliemann J.-O., Binder K, Gärtner F., Klassen T., Kreye H. 2011. On parameter selection in cold spraying. Journal of Thermal Spray Technology. 20(6): 1161-1176.

[6] Wong W., Irissou E., Ryabinin A.N., Legoux J.-G., Yue S. 2011. Influence of helium and nitrogen gases on the properties of cold gas dynamic sprayed pure titanium coatings. Journal of Thermal Spray Technology. 20(1-2): 213-226.

[7] Wong W., Vo P., Irissou E., Ryabinin A. N., Legoux J.-G., Yue S. 2013. Effect of particle morphology and size distribution on cold-sprayed pure titanium coatings. Journal of Thermal Spray Technology. 22(7): 1140-1153.

[8] Ryabinin A. N., Irissou E., McDonald A., Legoux J.-G. 2012. Simulation of gas-substrate heat exchange during cold-gas dynamic spraying. International Journal of Thermal Sciences. 56: 12-18.

[9] McDonald M. G., Ryabinin A. N., Irissou E., Legoux J.-G. 2013. Gas-substrate heat exchange during cold-gas dynamic spraying. Journal of Thermal Spray Technology. 22(2-3): 391-397.

[10] Marrocco T., McCartney D.G., Shipway P.H., Sturgeon A.J. 2006. Production of titanium deposits by cold-gas dynamic spray: numerical modeling and experimental characterization. Journal of Thermal Spray Technology. 15(2): 263-272.

[11] Jodoin B., Raletz F., Vardelle M. 2006. Cold spray modeling and validation using an optical diagnostic method. Surface and Coatings Technology. 200: 4424-4432.

[12] Klinkov S.V., Kosarev V.F., Sova A.A., Smurov I. 2009. Calculation of particle parameters for cold spraying of metal-ceramic mixtures. Journal of Thermal Spray Technology. 18(5-6): 944-956.

[13] Katanoda H., Fukuhara M., Iino N. 2007. Numerical study of combination parameters for particle impact velocity and temperature in cold spray. Journal of Thermal Spray Technology. 16(5-6): 627-633.

[14] Champagne V.K., Helfritch D.J., Dinavahi S.P.G., Leyman P.F. 2011, Theoretical and experimental particle velocity in cold spray. Journal of Thermal Spray Technology. 20(3): 425-431.

[15] Suo X.K., Liu T.K., Li W.Y., Suo Q.L., Planche M.P., Liao H.L. 2013. Numerical study on the effect of nozzle dimension on particle distribution in cold spraying. Surface and Coatings Technology. 220: 107-111.

[16] Jen T.-C., Li L., Cui W., Chen O., Zhang X. 2005. Numerical investigations on cold gas dynamic spray process with nano- and microsize particles. International Journal of Heat and Mass Transfer. 48: 4384-4396.

[17] Li W.-Y., Li C.-J., Wang H.-T., Li C.-X., Bang H.-S. 2006. Measurement and numerical simulation of particle velocity in cold spraying. Journal of Thermal Spray Technology. 15(4): 559-562.

[18] Li W.-H., Liao H., Douchy G., Coddet C. 2007. Optimal design of a cold spray nozzle by numerical analysis of particle velocity and experimental validation with 316L stainless steel powder. Materials and Design. 28: 2129-2137.

[19] Karimi M., Fartaj A., Rankin G., Vanderzwet D., Birtch W., Villafuerte J. 2006. Numerical simulation of the cold gas dynamic spray process. Journal of Thermal Spray Technology. 15(4): 518-523.

[20] Samareh B., Dolatabadi A. A. 2007. Three-dimensional analysis of the cold spray process: the effects of substrate location and shape. Journal of Thermal Spray Technology. 16(5-6): 634-642.

[21] Schmidt T., Assadi H., Gartner F., Richter H., Stoltenhoff T., Kreye H., Klassen T. 2009. From particle acceleration to impact and bonding in cold spraying. Journal of Thermal Spray Technology. 18(5-6): 794-808.

[22] Ning X.-J., Wang Q.-S., Ma Z., Kim H.-J. 2010. Numerical study of in-flight particle parameters in low-pressure cold spray process. Journal of Thermal Spray Technology. 19(6): 1211-1217.

[23] Sova A., Grigoriev S., Kochetkova A., Smurov I. 2014, Influence of powder injection point position on efficiency of powder preheating in cold spray: numerical study. Surface and Coatings Technology. 242: 226-231.

[24] Yin S., Liu Q., Liao H., Wang X. 2014. Effect of injection pressure on particle acceleration, dispersion and deposition in cold spray. Computational Materials Science. 90: 7-15.

[25] Lupoi R., O'Neill W. 2011. Powder stream characteristics in cold spray nozzles. Surface and Coatings Technology. 206: 1069-1076.

[26] Sova A., Okunkova A., Grigoriev S., Smurov I. 2013. Velocity of the particles accelerated by a cold spray micronozzle: experimental measurements and numerical simulation. Journal of Thermal Spray Technology. 22(1): 75-80.

[27] Stoltenhoff T., Kreye H., Richter H.J. 2002. An analysis of the cold spray process and its coatings. Journal of Thermal Spray Technology. 11(4): 542-550.

[28] Fukumoto M., Terada H., Mashiko M., Sato K., Yamada M., Yamaguchi E. 2009. Deposition of copper fine particle by cold spray process. Materials Transactions. 50(6): 1482-1488.

[29] Alkhimov A.P., Kosarev V.F., Klinkov S.V. 2001. The features of cold spray nozzle design. Journal of Thermal Spray Technology. 10(2): 375-381.

[30] Kosarev V.F., Klinkov S.V., Alkhimov A.P., Papyrin A.N. 2003. On some aspects of gas dynamics of the cold spray process. Journal of Thermal Spray Technology. 12(2): 265-281.

[31] Ryabinin A.N. 2015. Calculation of the particle velocity in cold spray in the one-dimensional non-isentropic approach. ARPN Journal of Engineering and Applied Sciences. 10(6): 2435-2439.

[32] Henderson C.B. 1976. Drag coefficients of spheres in continuum and rarefied flows. AIAA Journal. 14(6): 707-708.

[33] ANSYS CFX-Solver Modeling Guide. Release 13.0. 2010. Canonsburg: ANSYS, Inc., 604 p.

[34] Barth T. J. and Jespersen D. C. 1989. The design and application of upwind schemes on unstructured meshes. AIAA Paper. 89-0366:1-12.

[35] Menter F. R. 2009. Review of the shear-stress transport turbulence model experience from an industrial perspective. Int. J. of Computational Fluid Dynamics. 23(4): 305-316.